Journal of the European Ceramic Society 21 (2001) 907–917

www.elsevier.com/locate/jeurceramsoc

Thermomechanical properties and fracture mechanisms of calcium hexaluminate

Cristina Domínguez [a,*], Jérôme Chevalier [a], Ramon Torrecillas [b], Laurent Gremillard [a], Gilbert Fantozzi [a]

[a] *GEMPPM-UMR 5510, INSA de Lyon, bât. 502, 69621 Villeurbanne Cedex, France*
[b] *INCAR, CSIC, Ap. 73, 33080 Oviedo, Spain*

Received 15 June 2000; received in revised form 6 September 2000; accepted 21 September 2000

Abstract

Calcium hexaluminate is a material close to alumina which is recently being the subject of an increasing number of papers. However until now, nobody has deeply studied its properties or the mechanisms responsible for its mechanical behaviour. The flexural strength, toughness, crack growth resistance and thermal shock behaviour of calcium hexaluminate have been investigated. The observation of crack surfaces and cracks generated by indentation has allowed to identify the fracture mechanisms and to evaluate the influence of microstructure. Properties were compared to alumina. © 2001 Elsevier Science Ltd. All rights reserved.

Keywords: $CaO–6Al_2O_3$; Crack growth; Fracture; Mechanical properties; Thermal shock resistance

1. Introduction

Calcium hexaluminate ($CaAl_{12}O_{19}$ or $CaO{\cdot}6Al_2O_3$), often denoted as CA_6, occurs in nature as the mineral hibonite.[1] This phase is the most alumina-rich intermediate compound of the $CaO–Al_2O_3$ system,[2] and the one which exhibits the most excellent thermal properties.[3] CA_6 has a theoretical density[4] of 3.79 g/cm^3, crystallises in the hexagonal system (spacegroup $P6_3/mmc$),[4–6] and presents the structure of magnetoplumbite.

The morphology of CA_6 grains show preferential growth along their basal plane.[7,8] This growth-rate anisotropy is responsible both for the orientation of CA_6 with basal planes perpendicular to the reaction front,[7,9,10] and for the platelet or platelike (to classify grain shapes, the terms defined by Song et al.[11] for alumina grains are used) grain morphologies when CA_6 is obtained by reaction sintering.[12,13] On the contrary, when CA_6 is synthesised and milled previously to be pressed and sintered, grains are always equiaxed.[13,14] It is necessary to differentiate between grain growth during and after CA_6 formation, because both processes will contribute to final texture.[15] The morphology of CA_6 grains is related to the free space they have to develop during CA_6 formation, since their growth along their basal plane is limited by the presence of others grains. When the plates impinge upon each other, the grain growth proceeds at a much lower rate and the flat boundaries become curved. So, sometimes CA_6 obtained by reaction sintering can also present equiaxed morphologies.[12,15,16] After CA_6 formation, the main mechanism responsible for grain growth is the welding of neighbouring platelet grains when they are disposed with their flat boundaries, and thus with their basal planes, parallel.[15] For this reason, platelet grains become more equiaxed as firing temperature increases. When grains are equiaxed, the proportion of grains with basal planes parallel is very low, so the increase in firing temperature does not much affect grain granulometry. Fig. 1 illustrates the presence of both mechanisms: grain impingement and plates welding.

Some studies have been published concerning the mechanical properties of calcium hexaluminate, but in the majority of cases they are dedicated to the $CA_6–Al_2O_3$ composites.[17–24] The published properties of pure CA_6[13,14] present a high spread due to the differences in density and microstructure mainly caused by the different processing methods employed. The values reported

* Corresponding author. Tel.: +33-7243-8382; fax: +33-7243-8528.
E-mail address: jerome.chevaleir@insa-yon.fr (C. Domínguez).

PII: S0955-2219(00)00274-0

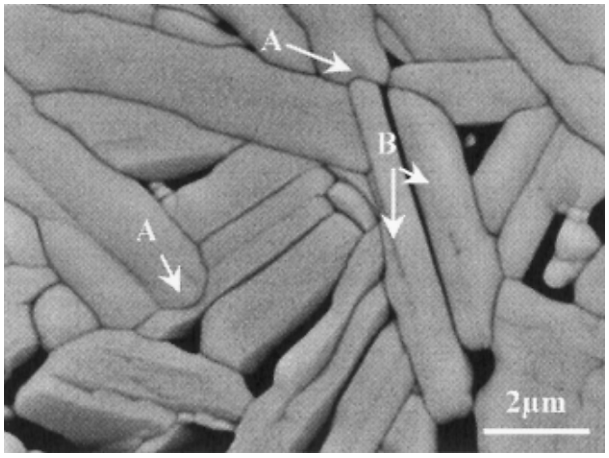

Fig. 1. SEM micrography at high magnification of a CA_6 sample obtained by reaction-sintering after firing at 1650°C a mixture of Al_2O_3 and $CaCO_3$. (A) It shows how growth is clamped by the neighbouring grains and (B) how the grains weld when they are disposed with their basal plane parallel and stuck together.

for the flexural strength and toughness at room temperature differ between 159–289 MPa and 3.2–4.5 MPa$\sqrt{m}$ for a pressureless sintered material, and 593–612 MPa and 3.0–3.4 MPa$\sqrt{m}$ for a hot pressed material. The works about the CA_6–Al_2O_3 composites show sometimes contradictory results. These works can be classified depending if they refer to alumina and alumina-spinel castables or to technical ceramics. Calcium hexaluminate is a reaction product in alumina and alumina-spinel castables that enhances their mechanical properties[25–27] thanks to the strong bond between CA_6 and alumina or spinel grains. Nevertheless some studies show just the opposite, that is, a continuous decrease in flexural strength as CA_6 proportion increases.[18] In the studies about CA_6–Al_2O_3 technical ceramics some authors show that the addition of CA_6 has any influence on toughness[22] while the majority founds higher K_{IC} values when CA_6 is added to Al_2O_3.[17,19–21,23] It has been shown that the increase in aspect ratio of CA_6 grains increases the crack growth resistance,[19–21] and that the crack morphology is planar when CA_6 grains are equiaxed, and tortuous when they are plates. They consider that the later behaviour is due to grain bridging. Fracture mechanism has been studied in CA_6 as fibre coating. This material cleaves across basal planes,[24] so cracking of CA_6 plates occurs more easily across plains parallel to its length. This cleavage will condition its mechanical behaviour.

The recent interest in the processing of ceramics whose microstructure exhibits platelike morphologies, has arisen in great part due to the fact that elongated grains can act as bridging sites in the wake of a crack, hence resulting in improved mechanical behaviour. Between magnetoplumbites that present this kind of morphology, CA_6 has been chosen as a reinforcing material in alumina composites[16–23] due to both its chemical compatibility and its mechanical and thermal expansion properties. Its easy cleaving crystallographic basal planes can be oriented parallel to a fibre-matrix interface making CA_6 a suitable material as alumina fibre coatings.[24,28,29] It presents a low solubility in iron containing slags[30–33] and a high stability in reducing atmospheres. These properties allow CA_6 to be in contact with steel and iron at high temperature without significant corrosion of the ceramic material. Hexaluminates can retain a large surface area at elevated temperature and can be good candidates as support materials for high temperature catalytic processes.[8,34,35] Thanks to the capacity of magnetoplumbites to accommodate fission product as Sr, Ba, Cs, and Ce in their structure,[36–39] their high chemical stability and low sensibility to radiation,[40,41] they are good host structures for long term immobilisation of nuclear waste.[42,43]

Despite the interesting potential applications of CA_6, up to date, only a few investigations regarding their mechanical properties have been reported with highly spread and contradictory results. This work focused on the study of some mechanical properties of calcium hexaluminate and the mechanisms responsible for its mechanical behaviour. Creep will be the subject of a next paper.

2. Experimental procedure

CA_6 was formed by reaction sintering of a mixture of 85.9 wt.% alumina (CT3000SG, Alcoa, Pittsburgh, Pennsylvania) and 14.1 wt.% calcium carbonate powders (PG-40, Asturcal, Gijon, Spain). Samples with different densities and microstructures were prepared by means of different processing methods. Details of processing methods employed, and microstructural and physical properties are reported elsewhere.[15] They are briefly presented in Table 1 and Fig. 2. As already reported in Ref. 15, it is difficult to reach full density in reaction sintered CA_6: even increasing sintering temperature up to 1750°C, i.e. slightly below the fusion temperature of pure hibonite, the density was only 95% of theoretical density. Thus samples were always quite porous. Hot pressing could have been used to process fully dense materials, but it leads to significant anisotropy of microstructure and properties, which complicates the analysis. Microstructure and properties of hot pressed CA6 will be the subject of a further paper.

Mechanical tests were conducted in bending on bar-shaped specimens with dimensions of about 4×6×40 mm^3. The tensile face of the flexural strength specimens and the largest faces of thermal shock specimens were polished with diamond paste (6 μm) and the edges were chamfered (about 45°). A straight notch was introduced, at the centre of the tensile face of specimens for toughness and R-curve tests, by means of a diamond

Table 1
Processing conditions, density and grains morphology of CA_6 samples

Sample	Processing conditions			Grains morphology				
	Mixing method	Forming method	Firing temperature (°C)	Bulk density (%)	Length (μm)	Width (μm)	Aspect ratio	Porosity distribution
SP	Stirring	Cold isostatic	1650	73.5±0.1	4.2±2.4	1.2±0.8	4.3±3.5	Wide size pores
		Pressing	1750	86.2±0.5	6.5±3.5	2.5±1.5	2.9±1.5	
AC	Attrition milling	Slip casting	1600	70.1±1.2	2.6±1.5	1.1±0.6	2.6±1.5	Homogeneous small pores
			1650	76.5±0.7	3.0±1.7	1.2±0.6	2.6±1.6	
			1700	88.3±0.8	3.2±2.1	1.3±0.9	2.7±1.7	
			1750	94.6±0.2	3.4±1.8	1.5±0.8	2.6±2.1	

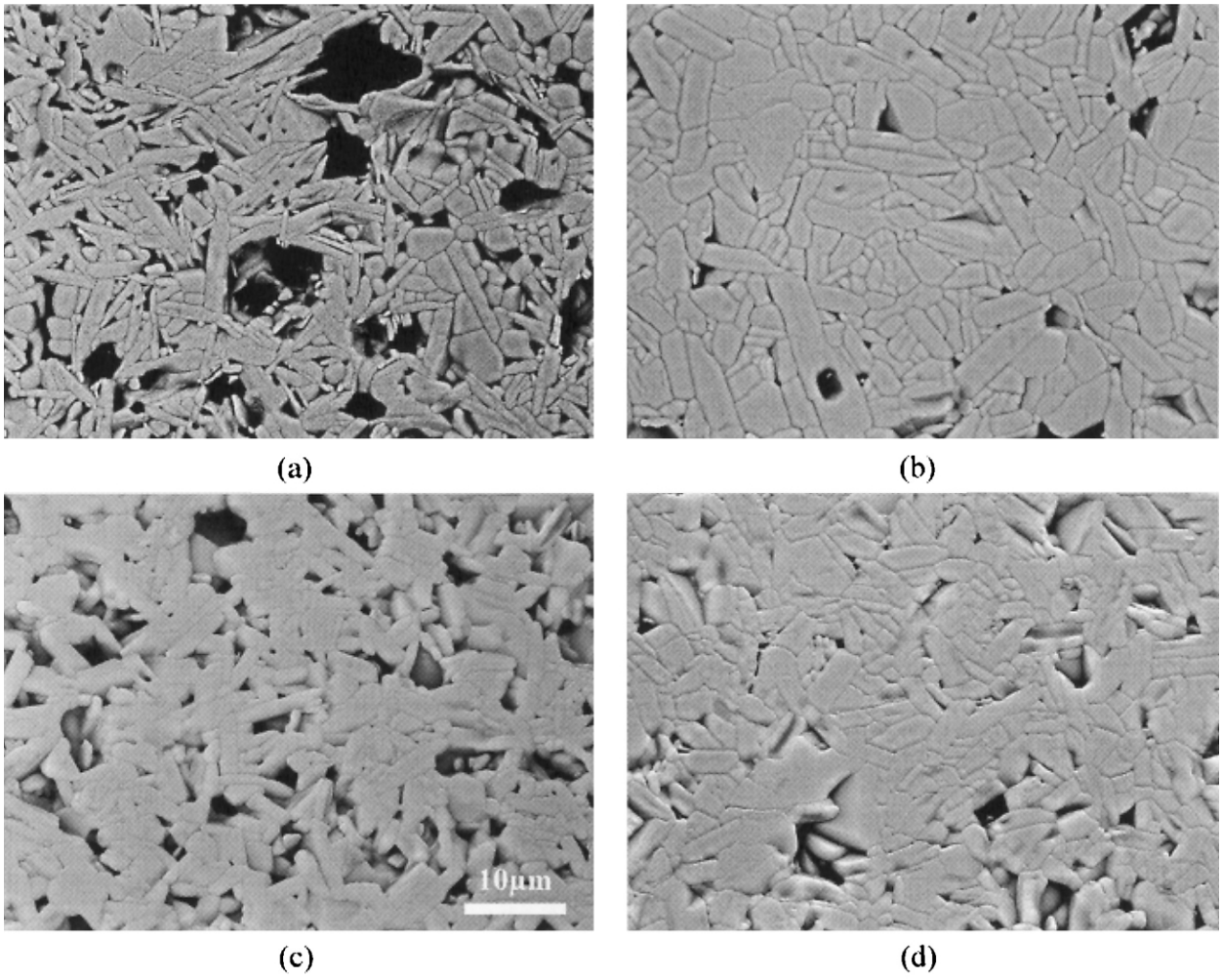

Fig. 2. SEM images of (a) SP and (c) AC samples fired at 1650°C and (b) SP and (d) AC samples fired at 1750°C. Note the higher aspect ratio of (a) in comparison with the other samples.

saw with a slot width of 0.3 mm. A second notch (diameter of about 70 μm) was carefully and slowly introduced by a razor sprinkled with a 6 μm diamond paste in correspondence of the tip of the first notch. The relative crack total length, a/W, was fixed at 0.3 and 0.55 for the toughness and R-curve tests respectively. Five specimens were used for the flexural strength, three for the toughness, one for the R-curve and a minimum of eight for the thermal shock tests.

Fracture tests were carried out with a four-point alumina device with an outer span of 35 mm and an inner span of 10 mm. The cross-head speed was 5 mm/min, except 3 μm/min for *R*-curve tests. Flexural strength and toughness were measured at room temperature,

1000, 1200 and 1400°C. The fracture toughness was determined using single edge notched beam (SENB) specimens. From the room temperature strength distribution and toughness mean values, the critical size distribution was evaluated according to:

$$K_{IC} = Y\left(\frac{a}{w}\right)\cdot\sigma_R\cdot\sqrt{a} \quad (1)$$

where K_{IC} is the toughness, σ_R the flexural strength, a the critical crack size and $Y(a/w)$ is the geometrical expression given by Tada et al.[44] The resistance to crack propagation was only measured at room temperature. The *R*-curve is determined during crack propagation from the measurement of the stress intensity factor, K_R, as a function of crack length. The crack length is determined indirectly from the load–displacement curve by the compliance method.[45] This method underestimates K_R values,[46] but is the only applicable due to the high porosity of most samples.

Details of the thermal shock test method have been described previously.[47] The specimens were initially heated in a resistance furnace at different temperatures for 10 min. and cooled symmetrically by the application of two jets of pulsed air to the largest faces. The acoustic emission (AE) of the sample was monitored by a piezoelectric transducer connected to a wave-guide in a discret contact with the specimen. The emissive response during cooling was recorded in order to detect the crack formation. The damage induced by thermal shock was characterised by measuring the evolution of the retained strength after crack detection.

To observe cracks path, sintered samples were cut and polished with a series of diamond pastes down to 6 μm. The polished samples were thermally etched at 1500°C for 1 h to release machining residual stresses, and indented at 200 N with a Vickers indenter. Finally indented samples and crack surfaces were gold coated for scanning electron microscopy observation (SEM) and energy dispersive X-ray microanalysis (EDX). Thin slices of materials were cut with a diamond wire, mechanically pre-thinned, and ion-milled for high-resolution transmission electron microscopy examination (HRTEM).

The main study was made using samples fired at 1650 and 1750°C, while the flexural strength of AC material was also measured after firing at 1600 and 1700°C in order to see the influence of porosity amount.

3. Results

Any glassy phase was observed by TEM, neither at grain boundaries, nor at triple joints. Nevertheless, inside the grains, it was seen the evidence of high dislocation activity, as shown in Fig. 3. The dislocations are located in bands of planes parallel to flat boundaries. At each side of these bands, the material has the same orientation, and dislocation planes are also parallel to one of the crystallographic planes of CA_6. As it was seen before, flat boundaries develop parallel to CA_6 basal planes, meaning that dislocation planes are also parallel to crystallographic basal planes.

Fig. 4 shows the flexural strength of different materials, σ_R, at room temperature, as a function of firing temperature. It can be observed that values as high as 380 MPa can be obtained, even if densities are never higher than 95%. The flexural strength of a ceramic material is linked to both its density and pores morphology. Usually, an increase in firing temperature leads to an increase in density and accordingly in flexural strength. This behaviour is followed only by AC samples, while in SP specimens σ_R decreases slighly as firing temperature increases. The evolution of σ_R as a function of total porosity is displayed in Fig. 5. For the same porosity values, SP samples have always a lower flexural strength than AC ones. The common behaviour is the decrease in σ_R as porosity rate increases, but SP material shows a slight increase with porosity. Only $\sigma_R = f(p)$ values of AC material can be fitted by a classical exponential law on the form:

$$\sigma_R = 430.e^{-2.6}p \quad (2)$$

where p is porosity.

Fig. 6 presents the toughness, K_{IC}, as a function of firing temperature. K_{IC} increases with firing temperature mainly due to the decrease in materials porosity. Thanks to the platelet microstructure of CA_6, a strengthening was expected due to a bridging mechanism, as it is usually observed in other platelet ceramic materials, but the material with higher aspect ratio (SP) is the one who shows the lower toughness values. This fact means that either bridging mechanisms are weak, or the low density of this material hides any strengthening effect.

Flexural strength is not an intrinsic parameter of a material, since it depends on the flaws present in the specimen. So the critical flaw sizes were measured. That of AC specimens (Fig. 7) does not change significantly with firing temperature. On the contrary, in SP samples, the critical flaw size grows up to about 100 μm when firing temperature increases to 1750°C.

The evolution of flexural strength as a function of test temperature is shown in Fig. 8. The σ_R decrease is more important in the samples that show high values at room temperature, so at 1400°C, the differences are small. It can also be observed that, in the temperature interval from 1000 to 1200°C, σ_R decreases significantly. Outside this temperature interval, the σ_R decrease is less important. As regard the toughness evolution as a function of test temperature (Fig. 9), it is similar in all tested materials, and almost constant between 1000 and 1400°C.

Fig. 10 shows the evolution of crack growth resistance, K_R, at room temperature with increasing crack

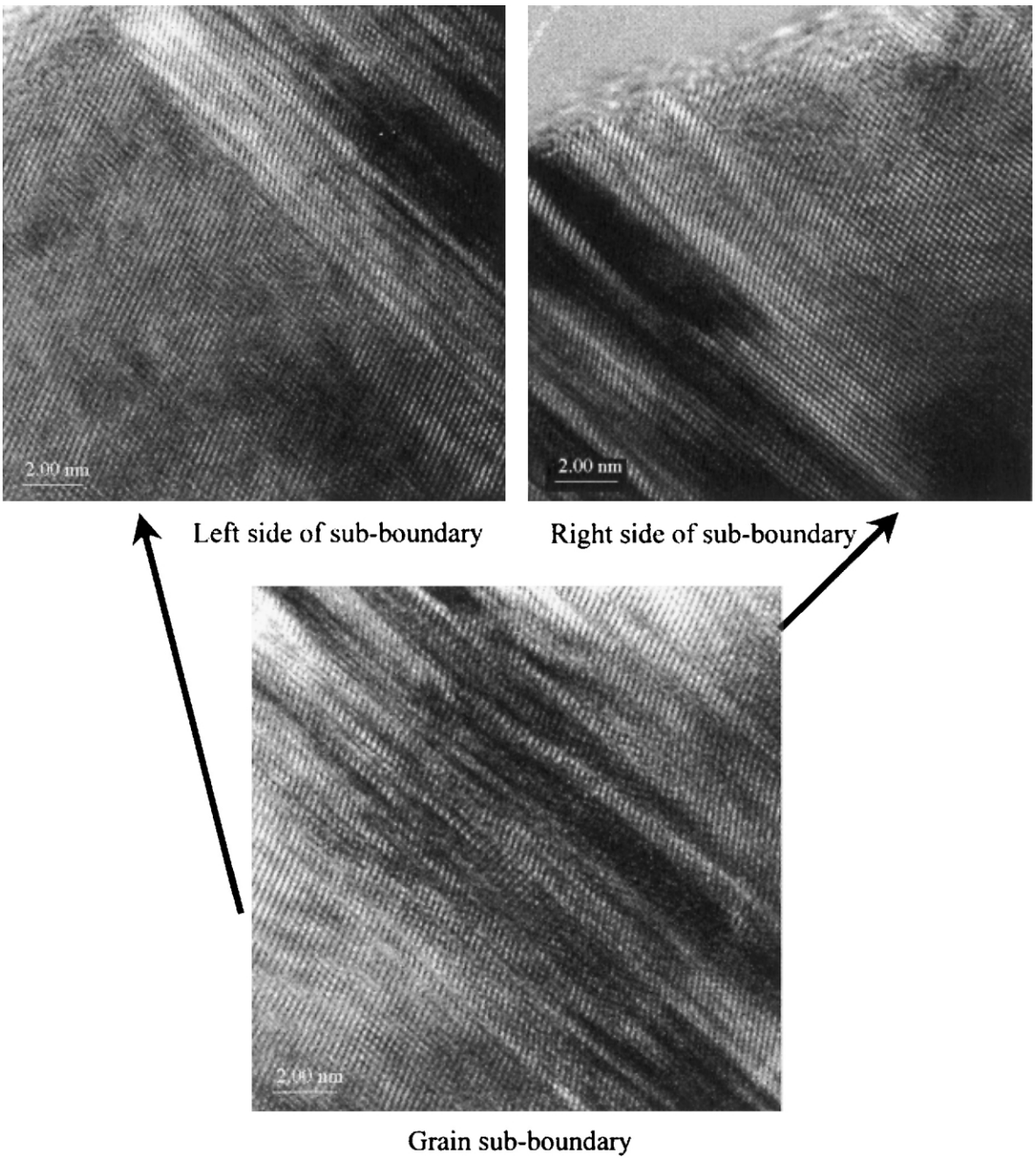

Fig. 3. TEM image of the bulk of a calcium hexaluminate grain.

length. K_R increases mainly in materials fired at 1750°C while those fired at 1650°C show any *R*-curve effect.

The crack surfaces of materials fired at 1750°C and tested at high temperature show the presence of tiny hexagonal plates on some grain boundaries, as shown in Fig. 11. These hexagonal plates are also composed of CA_6. This isolated fact is found only in materials fired at 1750°C, and after high temperature mechanical tests.

To better understand the mechanical behaviour of calcium hexaluminate, we decided to observe crack surfaces by SEM and to indent flat samples in order to follow crack paths. A typical crack surface of CA_6 is displayed in Fig. 12. It can be seen that cracking is mostly due to transgranular cleavage. The arrow shows a good example of "cleavage steps".

Fig. 13 shows the typical path followed by an indentation crack in an specimen of AC material fired at 1750°C. This path is complex and particularly sinuous. The crack goes through some grains boundaries (A points), but it propagates preferably through grains, and principally by planes parallel to flat boundaries (B points). Sometimes, and mainly in materials fired at 1750°C, crack can deflect to cross the grains by its larger dimension (C point). Any crack bridging was observed.

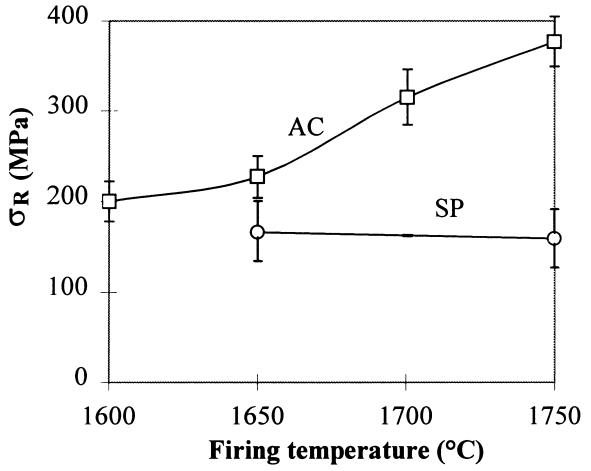

Fig. 4. Flexural strength at room temperature as a function of firing temperature.

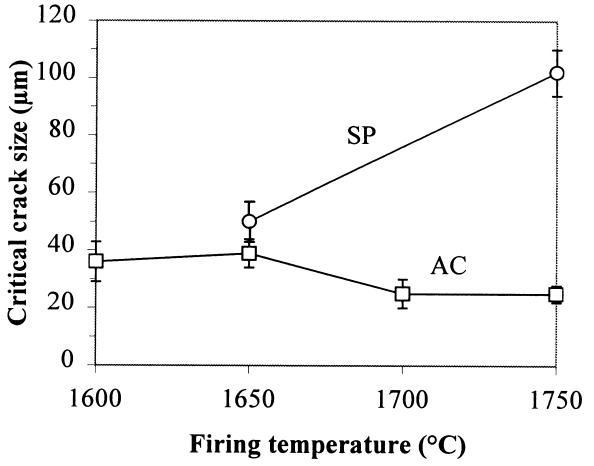

Fig. 7. Critical crack size evolution as a function of firing temperature.

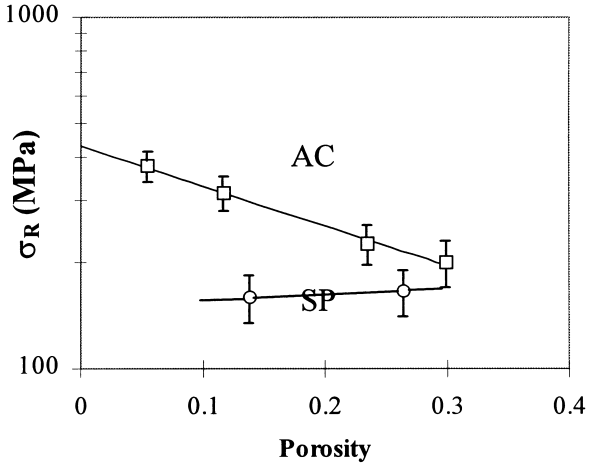

Fig. 5. Flexural strength evolution as a function of porosity.

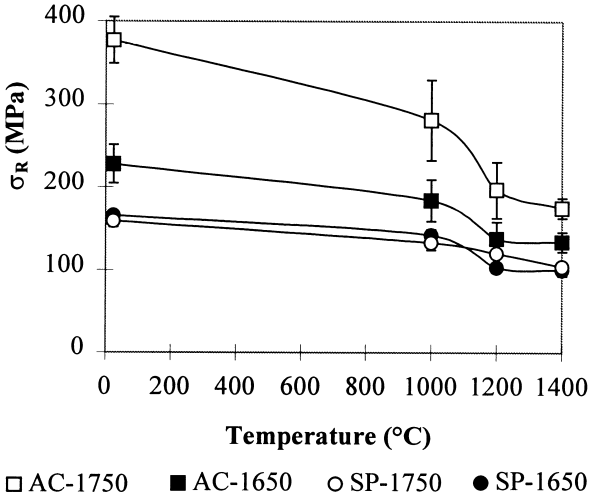

Fig. 8. Flexural strength evolution as a function of temperature.

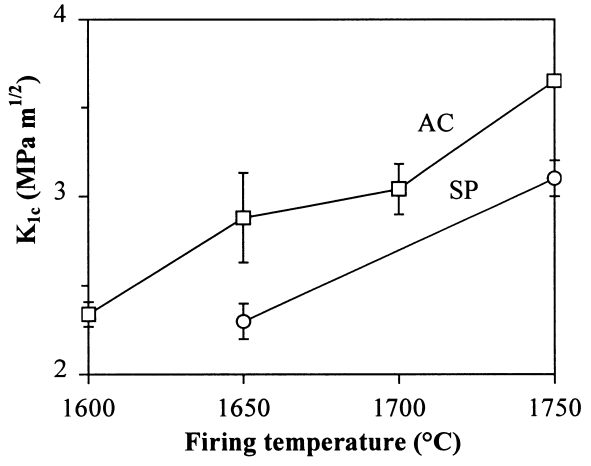

Fig. 6. Toughness at room temperature as a function of firing temperature.

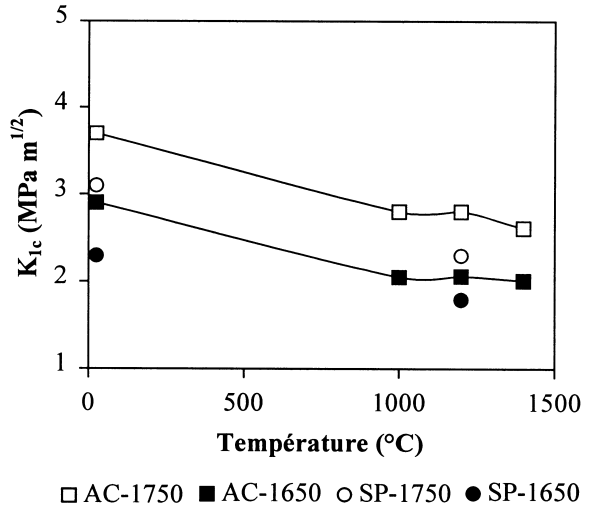

Fig. 9. Temperature dependence of toughness.

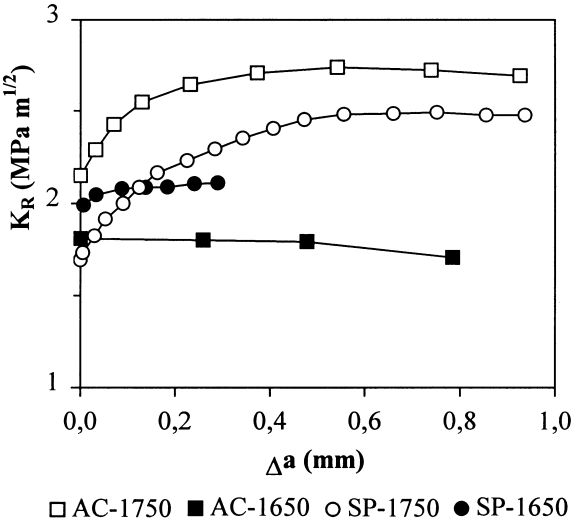

Fig. 10. Crack growth resistance.

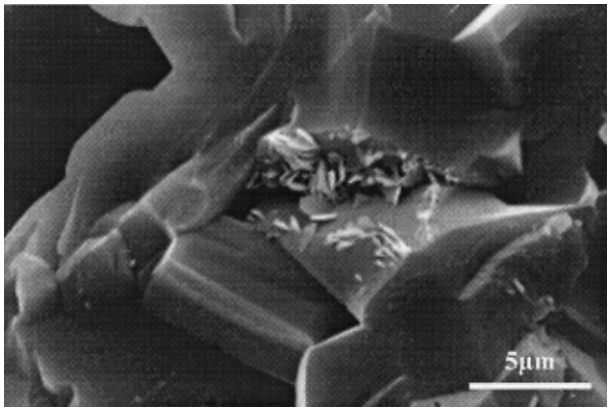

Fig. 11. Detail of crack surface of a SP specimen fired at 1750°C after a fracture test at 1000°C.

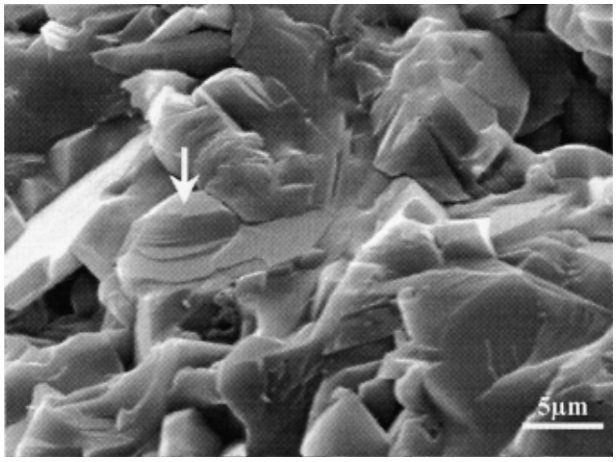

Fig. 12. SEM image of a typical crack surface of materials SP and AC.

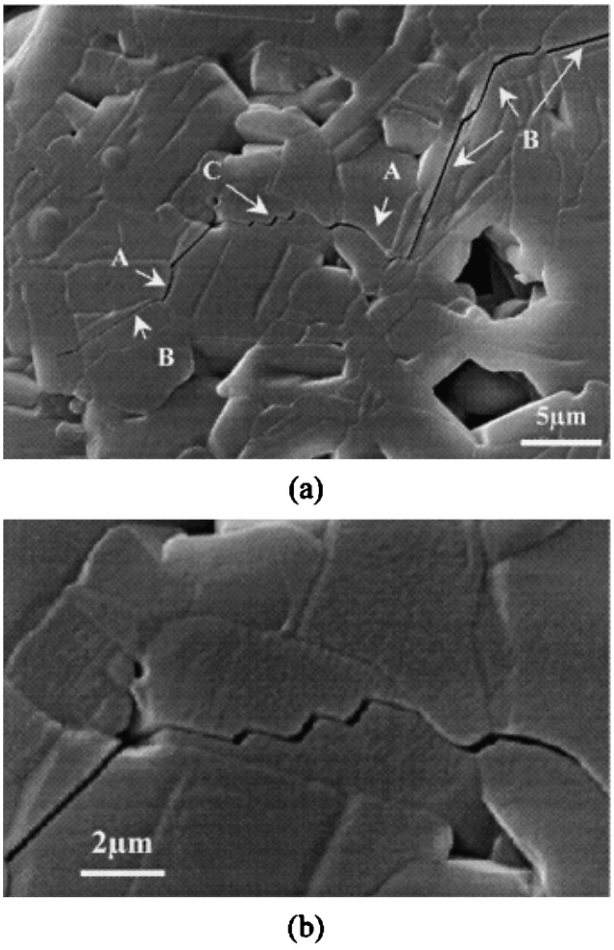

Fig. 13. (a) Crack path followed by an indentation crack in AC material fired at 1750°C: A, intergranular fracture; B, transgranular fracture without crack deviation; C, transgranular fracture with crack deviation. (b) Detail of C.

Thermal shock degradation, evaluated in terms of critical temperature and retained strength is represented in Table 2. Critical temperature is the temperature at which a sudden drop in strength appears due to the catastrophic propagation of incipient cracks. The lost of strength after thermal shock is an indicator of the extent of crack propagation. Material SP fired at 1650°C shows a strong fall off of strength (86%) as temperature reaches 550°C. When fired at 1750°C this materials presents a smaller fall off (49%) at a lower temperature. Material AC shows a similar behaviour, when fired at 1650°C its retained strength exhibits a strong degradation as temperature reaches 610°C, similar to that of material SP fired at the same temperature. Material AC also presents a smaller fall off (67%) at a lower temperature when fired at 1750°C than when fired at 1650°C. To sum up, critical temperature is higher in materials fired at 1650°C than in those fired at 1750°C. On the contrary, the retained strength is higher in materials fired at 1750°C.

4. Discussion

Even if any glassy phase was observed by TEM, a very small quantity of glassy phase must be present in

materials fired at 1750°C. The reason is the presence of tiny CA_6 plates on some grain boundaries in materials tested at high temperature (Fig. 11). It is indeed known that silica is rejected by CA_6 and accumulates at grain boundaries or triple points,[9,48] giving a silica and CA_6 rich glassy phase. During cooling, some CA_6 nucleation germs form from this glassy phase. During mechanical test at high temperature, these germs can grow to give the small CA_6 plates observed in Fig. 11.

As has been reported before,[15] the main mechanism responsible for the growth of calcium hexaluminate grains is the welding of neighbour grains when they are disposed with their basal planes parallel. Transmission electron microscopy showed the presence of dislocations at the interface between plates of the same orientation (Fig. 3). This fact shows that grain boundaries do not completely disappear during grain growth, and that a band of several dislocation planes appears instead, leading to the formation of many sub-boundaries inside grains. These sub-boundaries are parallel to basal plane in CA_6 grains.

Therefore, sub-boundaries can be seen as a preferential path to crack propagation. It was seen that the fracture is mainly transgranular across planes parallel to flat boundaries (Fig. 13). These planes can been identified as either basal planes or sub-boundaries. If crack deflects between sub-boundaries to cross the grains, it will lead to a larger distance between cleavage steps than when it deflects between basal planes. The height of steps showed in Fig. 13, larger than those observed in Fig. 12, can be interpreted as a sub-boundaries cracking. Usually in platelet microstructures an important grain bridging is observed. In calcium hexaluminate any grain bridging was noticed, but the high crack deflection observed instead will strengthen the material. This transgranular fracture along sub-boundaries means that the fracture energy of sub-boundaries is low, on the same order of the fracture energy for real grain boundaries (we shall remember that sub-boundaries correspond to the initial boundaries between plates of smaller dimensions). Thus, it is easier for the crack to propagate straight through the grains than along the grain boundaries, where long scale deviation is needed.

As has been seen in Fig. 5, only the flexural strength of AC samples can be related to the porosity. Flexural strength is not an intrinsic parameter of a material, since it depends on the flaws present in the specimen tested. The critical flaw size of AC specimens (Fig. 7) does not change significantly with firing temperature. On the contrary, in material SP, it grows up to about 100 μm when firing temperature is increased to 1750°C. A previous work of present authors showed that in low-density specimens (SP) pores have a wide size distribution and pores size can attempt 50 μm.[15] It is well known that the tendency of large pores during a densification process is to grow while that of small ones is to shrink and disappear.[49] In SP material, the slight increase in density with firing temperature is due to the size reduction of small pores, while bigger pores remain in the microstructure and even increase in size. As both pores size and critical flaw size of SP specimens grow up when firing temperature increases, it can be considered than in this material pores are the critical flaws. The grow up of critical flaw size when firing temperature increases explains the flexural strength decrease observed, in SP specimens, at high firing temperatures. Microstructure seems to do not play a direct role on CA_6 flexural strength because this property is mainly controlled by density and pores size. Therefore, to increase σ_R, it is necessary to optimise processing in order to decrease flaw size and increase density. Nevertheless, it is possible that a certain strengthening is produced in materials fired at 1750°C, those which present the higher σ_R values. At high temperature some grain boundaries disappear to form the sub-boundaries. These sub-boundaries will be stronger than the original grain boundaries.

σ_R shows an important degradation as test temperature increases in the temperature interval from 1000 to 1200°C (Fig. 8). This degradation is more important in AC sample fired at 1750°C. The materials fired at this temperature present at 1000°C a punctual crystallisation of glassy phase. The formation of small crystal can generate stresses and microcracks that can be responsible of this σ_R fall off observed at temperatures close to 1000°C. Outside the 1000–1200°C interval, the σ_R decrease follows a typical law of decrease in atomic bonding energies with temperature.

Usually, in platelet materials, grain bridging and crack deflection are the strengthening mechanisms. Thanks to the platelet microstructure of CA_6, a high strengthening was expected due to a bridging mechanism, and therefore a high crack growth resistance behaviour, but it has be shown that the material with the more equiaxed grains is the one who shows the higher toughness values and the only with a real *R*-curve effect. In fact, crack resistance is controlled by another mechanism. The crack predisposition to propagate along the basal planes or sub-boundaries, that produce high crack deflections, will strengthen the material. Again higher values of toughness and crack growth resistance are obtained in materials fired at 1750°C, even if grains seem equiaxed.

Retained strength after thermal shock (Table 2) is higher in materials that present a rising *R*-curve behaviour. Materials fired at 1750°C present a certain crack growth resistance, contrary to those fired at 1650°C, explaining the higher retained strength values of the former. The higher critical temperature of materials fired at 1650°C can be explained by their higher porosity, that induces a lower Young modulus and consequently lower thermal stresses.

Calcium hexaluminate is a material close to alumina, so their properties can be compared. Comparison is

Table 2
Critical temperature and retained strength after thermal shock in air for CA_6 materials

	SP		AC	
	1650°C	1750°C	1650°C	1750°C
T_c	550	470	610	500
σ/σ_0	0.14	0.51	0.13	0.33

quite delicate, specially as regard toughness measurement, because values are highly dependent of the employed method. Indentation methods must be avoid because they overestimate toughness in highly porous materials.[50,51] Notch diameter in SENB specimens has also an important influence. Usually, notch diameters as high as 0.2–0.3 mm are used, leading to a overestimate of toughness.[52,53] In this work notch diameters of 70 μm were used, that will give results closer to true K_{IC}. Calcium hexaluminate and alumina materials exhibit similar flexural strength and toughness values when density and grains size are similar.[54] It can even be higher in CA_6 at high porosity rates. At high temperatures flexural strength values of both materials are comparable[55] while toughness can be higher in CA_6. An alumina material with a similar grain size rarely exhibits an *R*-curve behaviour or it is very small,[56] so calcium hexaluminate can present a better crack growth resistance. Generally, alumina has a better thermal shock resistance that CA_6, showing both higher critical temperature and retained strength.[57–58] The main reason of this behaviour is the low thermal conductivity of CA_6, between 6 and 8 times lower than alumina at room temperature, and about a half at 1000°C.[59]

5. Conclusions

Until now, calcium hexaluminate was a material not fully characterised, as regards to its properties. A quite complete mechanical study has been done in order to understand the mechanisms responsible of its mechanical behaviour and to evaluate the influence of microstructure.

Calcium hexaluminate exhibits a flexural strength and toughness comparable to alumina at similar porosity. They can even be higher in CA_6 at high porosity rates. At high temperatures flexural strength values of both materials are similar while toughness can be higher in CA_6. Grain morphology seems to do not play an important role on CA_6 flexural strength because this property is mainly controlled by density and pores size. Nevertheless, it is possible that a certain strengthening is produced in materials fired at 1750°C, thanks to the disappearing of grain boundaries to form the subboundaries. Thanks to the platelet microstructure of CA_6, a high strengthening was expected due to a bridging mechanism, and therefore a high crack growth resistance behaviour, but any grain bridging was observed. Nevertheless fracture is controlled by another mechanism, that is, the crack predisposition to propagate along the basal planes or the sub-boundaries, that produces high crack deflections. This strengthening allows calcium hexaluminate to present a better crack growth resistance than alumina. Nevertheless, due to the lower thermal conductivity of CA_6, its thermal shock resistance is lower than in alumina, showing both lower critical temperature and retained strength.

As CA_6 is a "new" material, it is necessary to look for its potentialities. This material will be better than alumina for applications where it is necessary to have a porous, low thermal conductivity or high crack growth resistant material. It is also important to consider its high stability in reducing atmospheres and low solubility in iron containing slags. Nevertheless it is necessary to keep in mind its low thermal shock resistance. New applications for monolithic CA_6 could be in filters or thermal insulating, specially in insulating fibres because alumina ones show an important sintering at high temperatures, but the future of this material will be in alumina composites thanks to the higher crack growth resistance that it brings. This application would now be better developed thanks to the knowledge of mechanism that controls CA_6 behaviour.

References

1. Curien, H., Guillemin, C. and Orcel, J. et al., L'Hibonite, nouvelle espèce minérale. *Compt. Rend. Hebd. Seances Acad. Sci.*, 1958, **242**, 2845–2847.
2. Nurse, R. W., Welch, J. H. and Majumdar, A. J., The $CaO–Al_2O_3$ system in a moisture-free atmosphere. *Trans. Br. Ceram. Soc.*, 1965, **64**, 409–418.
3. Hallstedt, B., Assessment of the $CaO–Al_2O_3$ System. *J. Am. Ceram. Soc.*, 1990, **73**, 15–23.
4. Utsunomiya, A., Tanaka, K. and Morikawa et al., Structure refinement of $CaO·6Al_2O_3$. *J. Solid State Chem.*, 1988, **75**, 197–200.
5. Collongues, R., Gourier, D. and Kahn-Harari, A. et al., Magnetoplumbite related oxides. *Annu. Rev. Mater. Sci.*, 1990, **20**, 51–82.
6. Park, J. G. and Cormack, A. N., Potential models for multicomponent oxides — hexa-aluminates. *Philos. Mag. B*, 1996, **73**, 21–31.
7. Kohatsu, I. and Brindley, G. W., Solid state reactions between CaO and α-Al_2O_3. *Z. Phys. Chem., Neue Folge*, 1968, **60**, 79–89.
8. Machida, M., Shiomitsu, T., Inoue, H. et al., Hexaaluminate-related compounds as thermally stable catalyst materials. In *Ceramics Transactions, Vol. 31, Porous Materials,* ed. K. Ishizaki. Am. Ceram. Soc., 1993, pp. 273–282.
9. De Jonghe, L. C., Schmidt, H. and Chang, M., Interaction between Al_2O_3 and a $CaO–Al_2O_3$ Melt. *J. Am. Ceram. Soc.*, 1984, **67**, 27–30.
10. Moya, J. S., de Aza, A. H. and Steier, H. et al., Reactive coating on alumina substrates-calcium and barium hexaluminates. *Scrip. Metall. Mat.*, 1994, **31**, 1049–1054.
11. Song, H. and Coble, R. L., Origin and growth kinetics of platelike abnormal grains in liquid-phase-sintered alumina. *J. Am. Ceram. Soc.*, 1990, **73**, 2077–2085.

12. Dominguez, C. and Torrecillas, R., Influence of Fe^{3+} in the sintering and microstructural evolution of reaction dintered calcium hexaluminate. *J. Eur. Ceram Soc*., 1998, **18**, 1373–1379.
13. Criado, E., Pena, P. and Caballero, A., Influence of processing method on microstructural and mechanical properties of calcium hexaluminate Compacts. In *Science of Ceramics, vol. 14, Proceedings of the 14th International Conference Science of Ceramics. Inst. of Ceramics*, ed. D. Taylor. Shelton, Staffs, UK, 1988, pp. 193–198.
14. Nagaoka, T., Kanzaki, S. and Yamaoka, Y., Mechanical properties of hot-pressed calcium hexaluminate ceramics. *J. Mat. Science Lett*., 1990, **9**, 219–221.
15. Dominguez, C., Chevalier, J., Torrecillas, R. et al., Microstructure development of calcium hexaluminate. *J. Eur. Ceram. Soc*. 2001, **21**, 381–387.
16. An, L., Chan, H. M. and Soni, K. K., Control of calcium hexaluminate grain morphology in in-situ toughened ceramic composites. *J. Mat. Science*., 1996, **31**, 3223–3229.
17. Asmi, D. and Low, I. M., Physical and mechanical characteristics of in-situ alumina/calcium hexaluminate composites. *J. Mat. Science Lett*., 1998, **17**, 1735–1738.
18. Mendoza, J. L., Freese, A. and Moore, R. E., Thermomechanical behaviour of calcium aluminate composites. In *Ceramic Transactions Vol. 4, Advances in Refractories Technology*, ed. R. E. Fisher. American Ceramic Society, Westerville, OH, 1989, pp. 294–311.
19. An, L., Chan, H. M., Padture, N. P. and Lawn, B. R., Damage-resistant alumina-based layer composites. *J. Mater. Res*., 1996, **11**, 204–210.
20. An, L. and Chan, H. M., R-Curve behavior of in-situ-toughened Al_2O_3:$CaAl_{12}O_{19}$ ceramic composites. *J. Am. Ceram. Soc*., 1996, **79**, 3142–3148.
21. L. An, L., Hyoung-Chan, H. and Chan, H. M., High-strength alumina/alumina calcium hexaluminate layer composites. *J. Am. Ceram. Soc*., 1998, **81**, 3321–3324.
22. Criado, E., Caballero, A. and Pena, P., Microstructural and mechanical properties of alumina-calcium hexaluminate composites. In *High Tech Ceramics*, ed. P. Vincenzini. Elsevier Science publishers, Amsterdam, 1987, pp. 2279–2289.
23. Asmi, D., Low, I. M. and Kennedy, S. et al., Characteristics of a layered and graded alumina/calcium hexaaluminate composites. *Mat. Lett*., 1999, **40**, 96–102.
24. Cinibulk, M. K., Microstructure and mechanical behavior of an hibonite interphase in alumina-based composites. *Ceram. Eng. Sci. Proc*., 1995, **16**, 633–641.
25. Kopanda, J. E. and Maczura, G., Production processes, properties and applications for calcium aluminate cements. In *Alumina Chemical Science and Technology Handbook*, ed. L. D. Hart. Am. Ceram. Soc, Westerville, OH, 1990, pp. 171–184.
26. Teoreanu, I. and Muntean, M., Alumina refractory masses hardened at normal temperatures by coagulation, In *ECERS V, Key Engineering Materials,* Vols 132–136. Trans Tech Publications, Switzerland, 1997, pp. 1825–1828.
27. Chan, C. and Jo, Y., Effect of CaO Content on the hot strength of alumina-spinel castables in the temperature range of 1000° to 1500°C. *J. Am. Ceram. Soc*., 1998, **81**, 2957–2960.
28. Cinibulk, M. K. and Hay, R. S., Textured magnetoplumbite fiber-matrix intherphase derived from sol–gel fiber coatings. *J. Am. Ceram. Soc*., 1996, **79**, 1233–1246.
29. Cinibulk, M. K., Magnetoplumbite compounds as a fiber coating in oxide–oxide composites. *Ceram. Eng. Sci. Proc*., 1994, **15**, 721–728.
30. Buist, D. S., A study of calcium hexaluminate. *Mineralogical Mag*., 1968, **36**, 676–686.
31. Dayal, R. R. and Glasser, F. P., Phase relations in the system CaO–Al_2O_3–Fe_2O_3. In *Science of Ceramics, Vol. 3*, ed. G. H. Stewart. Academic Press, New York, 1967, pp. 191–214.
32. Lister, D. H. and Glasser, F. P., Phase relations in the system CaO–Al_2O_3-iron oxide. *Trans Brit. Ceram. Soc*., 1967, **66**, 293–305.
33. Imlach, J. A. and Glasser, F. P., Sub-solidus phase relations in the system CaO–Al_2O_3–Fe–Fe_2O_3. *Trans. J. Br. Ceram. Soc*., 1971, **70**, 227–234.
34. Arai, H. and Machida, M., Recent progress in high-temperature catalytic combustion. *Catalysis Today*, 1991, **10**, 81–94.
35. Machida, M., Teshima, T. and Eguchi, K. et al., High-temperature steam reforming of hidrocarbons over nickel/hexaaluminate catalysts. *Chem. Lett*., 1991, **2**, 231–234.
36. Collongues, R., Applications generales des phases de type alumine β et magnétoplombite. *Ann. Chim.-Science des Materiaux*, 1985, **10**, 385–396.
37. Thery, J., Vivien, D. and Lejus, A. M.etal., Les composés de type magnétoplombite et SLNA, materiaux pour le stockage d'elements radioactifs. *Ann. Chim.-Science des Materiaux*, 1985, **10**, 397–399.
38. Hench, L. L., Clark, D. E. and Harker, A. B., Review nuclear waste solids. *J. Mat. Sci*., 1986, **21**, 1457–1478.
39. Morgan, R. E. D., Clarke, D. R., Jantzen, C. M. and Harker, A. B., High-alumina tailored nuclear waste ceramics. *J. Am. Ceram. Soc*., 1981, **64**, 249–258.
40. Jantzen, C. M., Clarke, D. R. and Morgan, P. E. D. et al., Leaching of polyphase nuclear waste ceramics: microstructural and phase characterization. *J. Am. Ceram. Soc*., 1982, **65**, 292–300.
41. Troester, J. K., Freeborn, W. P. and White, W. B., Dissolution kinetics of magnetoplumbite. In *In Advances in Ceramics, vol. 8, Nuclear Waste Management*, ed. G. G. Wicks and W. A. Ross. Am. Ceram. Soc, Columbus, OH, 1984, pp. 247–254.
42. Harker, A. B. and Flintoff, J. F., Hot isostatically presses ceramic and glass forms for immobilizing hanford high-level wastes. In *In Advances in Ceramics, vol. 8. Nuclear Waste Management*, ed. G. G. Wicks and W. A. Ross. Am. Ceram. Soc, Columbus, OH, 1984, pp. 222–233.
43. Morgan, R. E. D. and Cirlin, E. H., The magnetoplumbite crystal structure as a radwaste host. *J. Am. Ceram. Soc*., 1982, **65**, C114–115.
44. Tada, H.Paris and Irwin, G. R., *The stress analysis of cracks handbook*, 2nd edn Del Research Corporation, St. Louis, MS, 1985.
45. Saadaoui, M., *Contribution à l'Étude du Comportement Thermomécanique des Matériaux Céramiques à Effet de courbe R : Choc et Fatigue Thermiques*. PhD thesis, Ecole Mohammadia d'Ingénieurs et Institut National des Sciences Appliquées de Lyon, 1996.
46. Ebrahimi, M., Chevalier, J., Saadaoui, M. et al., Effect of grain size on crack growth in alumina. In *Proceedings of VII Fracture Mechanics of Ceramics*, Moscou, 20–22 July 1999.
47. Mignard, F., Olagnon, C. and Fantozzi, G., Acoustic emission monitoring of damage evaluation in ceramics submitted to thermal shock. *J. Eur. Ceram. Soc*., 1995, **15**, 651–653.
48. Mallamaci, M. P., Sartain, K. B. and Carter, C. B., Crystallization of calcium hexaluminate on basal alumina. *Philosophical magazine A*, 1998, **77**, 561–575.
49. Halloran, J. W., Role of powder agglomerates in ceramic processing. In *Advances in Ceramics, vol. 9. Forming of Ceramics*, ed. J. A. Mangels and G. L. Messing. American Ceramic Society, Columbus, OH, 1984, pp. 67–75.
50. Anstis, G. R., Chantikul, P. and Lawn, B. R. et al., A critical evaluation of indentation techniques for measuring fracture toughness: I, direct crack measurements. *J. Am. Ceram. Soc*., 1981, **64**, 533–538.
51. Chantikul, P., Anstis, G. R. and Lawn, B. R. et al., A critical evaluation of indentation techniques for measuring fracture toughness: II, strength method. *J. Am. Ceram. Soc*., 1981, **64**, 539–543.
52. Nishida, T. and Hanaki, Y., Effect of notch-root radius on the fracture toughness of a fine-grained alumina. *J. Am. Ceram. Soc*., 1994, **77**, 606–608.

53. Primas, R.J. and Gstrein, R. ESIS TC6 Round robin on fracture toughness. EMPA report no. 155′088. Dübendorf. EMPA, 1995.
54. Dörre, E. H. and Hübner et al., *Alumina. Processing, Properties, and Applications*. Springer-Verlag, Berlin, 1984.
55. Munro, R. G., Evaluated material properties for a sintered α-alumina. *J. Am. Ceram. Soc.*, 1997, **80**, 1919–1928.
56. Chantikul, P., Bennison, S. J. and Lawn, B. R., Role of grain size in the strength and R-curve properties of alumina. *J. Am. Ceram. Soc.*, 1990, **73**, 2419–2427.
57. Mignard, F., *Etude du Comportement au Choc et à la Fatigue Thermiques de Céramiques pour Applications Industrielles*. PhD thesis, Institut National des Sciences Appliquées de Lyon, 1994.
58. Saadaoui, M. and Fantozzi, G., Crack growth resistance under thermal shock loading of alumina. *Mat. Sci. Eng. A*, 1998, **247**, 142–151.
59. Dominguez, C., *Formation, Microstructure et Propriétés de l'Hexaluminate de Calcium*. PhD thesis, Institut National des Sciences Appliquées de Lyon, 2000.